Genetics in Medicine
An Official Journal of the ACMG

ARTICLE

Bi-allelic *NIT1* variants cause a brain small vessel disease characterized by movement disorders, massively dilated perivascular spaces, and intracerebral hemorrhage

Julie W. Rutten[1],*, Minne N. Cerfontaine[1], Kyra L. Dijkstra[2], Aat A. Mulder[3],
Jeroen Vreijling[1], Mark Kruit[4], Roman I. Koning[3], Susanne T. de Bot[5],
Koen M. van Nieuwenhuizen[6], Hans J. Baelde[2], Henk W. Berendse[7], Leon H. Mei[8],
George J.G. Ruijter[9], Frank Baas[1], Carolina R. Jost[3], Sjoerd G. van Duinen[2],
Esther A.R. Nibbeling[1], Gido Gravesteijn[1], Saskia A.J. Lesnik Oberstein[1]

ABSTRACT

Purpose: To describe a recessively inherited cerebral small vessel disease, caused by loss-of-function variants in *Nitrilase1* (*NIT1*).

Methods: We performed exome sequencing, brain magnetic resonance imaging, neuropathology, electron microscopy, western blotting, and transcriptomic and metabolic analyses in 7 NIT1-small vessel disease patients from 5 unrelated pedigrees.

Results: The first identified patients were 3 siblings, compound heterozygous for the *NIT1* c.727C>T; (p.Arg243Trp) variant and the *NIT1* c.198_199del; p.(Ala68*) variant. The 4 additional patients were single cases from 4 unrelated pedigrees and were all homozygous for the *NIT1* c.727C>T; p.(Arg243Trp) variant. Patients presented in mid-adulthood with movement disorders. All patients had striking abnormalities on brain magnetic resonance imaging, with numerous and massively dilated basal ganglia perivascular spaces. Three patients had non-lobar intracerebral hemorrhage between age 45 and 60, which was fatal in 2 cases. Western blotting on patient fibroblasts showed absence of NIT1 protein, and metabolic analysis in urine confirmed loss of NIT1 enzymatic function. Brain autopsy revealed large electron-dense deposits in the vessel walls of small and medium sized cerebral arteries.

Conclusion: NIT1-small vessel disease is a novel, autosomal recessively inherited cerebral small vessel disease characterized by a triad of movement disorders, massively dilated basal ganglia perivascular spaces, and intracerebral hemorrhage.

Introduction

Genetic causes of intracerebral hemorrhage (ICH) are rare, and they all have an autosomal dominant pattern of inheritance. The most well-known gene associated with ICH is *APP,* causing hereditary cerebral amyloid angiopathy. *NOTCH3*, *COL4A1*, and *COL4A2* are other examples of genes causing cerebrovascular disorders in which ICH can occur, but with a much lower frequency.[1] Autosomal recessive forms of ICH have to the best of our knowledge never been reported.

The Nitrilase1 (NIT1) protein is a member of the nitrilase protein family. *NIT1* is highly conserved and is ubiquitously expressed in adult human and mouse tissues and during mouse embryogenesis.[2] The role of NIT1 in human health and disease has been incompletely clarified. Mouse studies have shown that NIT1 acts as a metabolite repair enzyme, hydrolyzing the deaminated form of the common intracellular antioxidant glutathione (dGSH).[3] Moreover, NIT1 has been suggested to act as a tumor suppressor via activation of the TGFβ–Smad and WNT signaling pathways.[2,4,5] In humans, there has only been 1 clinical report describing 3 brothers with bi-allelic *NIT1* loss-of-function variants and a psychiatric phenotype and cavities on brain magnetic resonance imaging (MRI).[6]

Here, we show that bi-allelic *NIT1* loss-of-function variants cause a genetic cerebral small vessel disease, resulting in a triad of movement disorders, massively dilated perivascular spaces on brain MRI, and fatal deep ICH. We describe the clinical phenotype, neuroimaging features, and brain vessel wall pathology of 7 patients from 5 unrelated Dutch pedigrees. Furthermore, we calculate minimal estimated NIT1-small vessel disease prevalence based on *NIT1* pathogenic variant frequencies in the Genome of the Netherlands database, the Genome Aggregation Database (gnomAD), and UK Biobank.

Materials and Methods

Ascertainment and study approval

The first ascertained family comprised 3 siblings with a distinct neuroimaging phenotype and ICH, leading to the suspicion of an autosomal recessive monogenic cause. Subsequently, 2 unrelated and isolated cases with a similar neuroimaging phenotype were recognized and 2 unrelated and isolated cases were identified after reanalysis of next-generation sequencing data of patients previously referred to the Leiden Laboratory for Diagnostic Genome Analysis because of suspected genetic small vessel disease. This study has been approved by the Medical Ethics Committee Leiden The Hague Delft (P21.013). Written informed consent for publication was obtained from 6 out of 7 patients.

Exome sequencing and 3D modeling

Genomic DNA was extracted from whole blood. Exome sequencing was performed on an Illumina platform after exome enrichment using the Agilent SureSelectXT Human All Exon v5, v7 or SureSelect Clinical Research Exome V2 kit at Genomescan B.V. Burrows-Wheeler Aligner was used for read alignment, and Genome Analysis Tool Kit was used for variant calling. Annotation was performed using in-house LUMC software using reference transcript NM_005600.2. Variants were classified according to ACMG guidelines,[7] and reported according to HGVS recommendations (http://varnomen.hgvs.org/). Copy-number analysis was performed in patients with homozygous variants (patients 4 and 5), to exclude a deletion on 1 of the alleles. 3D modeling was performed using AlphaFold,[8] and 3D models were visualized using ChimeraX (https://www.rbvi.ucsf.edu/chimerax/).

Brain MRI

For the 2 affected patients who participated in our on-site clinical study, brain MRI was performed on a 3 Tesla MR system (Philips Achieva TX, Philips Medical Systems), including the following sequences: 3-dimensional T1-weighted images, T2-weighted images, fluid-attenuated inversion recovery (FLAIR), and susceptibility-weighted images (SWI). For all other patients, clinical 1.5 tesla MRIs were available with the exception of 1 patient, who had only undergone a CT scan at the time of a massive hemorrhagic stroke. Brain MRIs were qualitatively assessed by M.N.C. and by M.K.

Immunohistochemistry and electron microscopy of brain vessels

Paraffin embedded brain tissue was available of 2 deceased siblings, frozen brain tissue was available of 1. Control brain tissue was obtained from 2 deceased individuals in whom autopsy was performed and tissue processed at the same pathology department as that of the patients. Brain tissue was sectioned and stained with Hematoxylin-eosin, Periodic acid-Schiff, Toloidine Blue, and Congo Red. Immunohistochemistry was performed using NOTCH3 (1E4, Millipore, dilution 1:1000), NIT1 (Ab180942, Abcam, dilution 1:50), and beta amyloid antibodies (Clone 6F/D3, Dako, dilution 1:20). Skin biopsies were obtained from 3 patients and 3 unaffected heterozygous family members and were processed for immunohistochemistry and electron microscopy. Electron microscopy was performed in brain tissue of the 2 deceased patients and in 2 skin biopsies. For electron microscopy, ultrathin sections (90 nm) were made on a Reichert Ultracut S (Leica Microsystems) and stained with uranyl acetate and lead citrate. Electron microscopy images were recorded with a Tecnai 12 transmission electron microscope (Thermo Fisher Scientific, formerly FEI). Overlapping images were automatically collected and stitched together into a virtual slide as previously described.[9]

Western blot and transcriptomics on patient fibroblasts and metabolic analysis in urine

Fibroblast cultures were obtained from skin punch biopsies according to standard diagnostic workup. In 2 independent experiments, protein was extracted using RIPA-buffer (25 mM Tris-HCl, 150 mM NaCl, 1% Nonident P40, 1% sodium-deoxycholate, 0,1% SDS, and 1× protease inhibitor Roche 04693132001), and the total protein concentration was measured using a BCA protein assay kit (Pierce No. 23227, Thermofisher). After sonication, 20 μg of protein was loaded per lane. Samples were separated using SDS-PAGE and transferred to a PVDF-membrane (No. 162-0177, Bio-Rad). Membranes were incubated overnight at 4°C with an anti-NIT-1 monoclonal rabbit antibody (Abcam, ab180942) at a 1:500 dilution and subsequently with an HRP-conjugated anti-rabbit IgG antibody (Agilent, P0448) for 1 hour at a 1:2000 dilution. Antigen was detected by chemiluminescence reaction (ECL Pierce, 32106, Thermofisher). An α-Tubulin monoclonal mouse antibody (Cell Signaling, 3873) was used as a loading control. RNA was isolated using the NucleoSpin XS RNA Kit (Machery-Nagel; Ref. 74090250), and RNA sequencing (RNA-seq) was performed at Genomescan B.V. on the NovaSeq6000. RNA-seq data were processed using the opensource BIOWDL RNA-seq pipeline v5.0.0 (https://doi.org/10.5281/zenodo.3459256). FastQC was used for quality control of raw reads, and adapter clipping was performed using Cutadapt (v2.10) with default settings. RNA-seq reads' alignment was performed using STAR (v2.7.5a) on the GRCh38 human reference genome. The gene read annotation and quantification was performed using HTSeq-count (v0.12.4), based on Ensembl version 109. PCA plots were created using the dgeAnalysis R package (GitHub - LUMC/dgeAnalysis: R package with Shiny application for DGE analysis).

Urine samples were obtained from 2 patients and 3 unaffected heterozygous family members. Analysis of urine organic acids, including the NIT1 substrate deaminated glutathione (dGSH),[3] was performed by gas chromatography-mass spectrometry of trimethylsilyl-derivatives.

Ascertainment of *NIT1* variants in UK Biobank

Details on the UK Biobank study have been described previously.[10] *NIT1* truncating variants (nonsense and frameshift variants) and the *NIT1* c.727C>T; p.(Arg243Trp) variant were ascertained in exome sequencing data of 454,805 UK Biobank participants, using reference transcript NM_005600.2. Of individuals with these *NIT1* variants, ICD10 codes and available brain MRIs were extracted. Brain MRI was available for 20 c.727C>T; p.(Arg243Trp) heterozygotes and for 42 individuals heterozygous for a truncating *NIT1* variant and was compared with 62 age- and sex-matched controls from UK Biobank.

Analysis of stroke frequency and MRI quantification in individuals heterozygous for a *NIT1* variant in UK Biobank

Ischemic and hemorrhagic stroke were assessed using ICD-10 codes (I61, I63, and I64). MRIs from UK Biobank were rated by an experienced observer (M.N.C.) blinded for genotype. Dilated perivascular spaces (dPVS) were evaluated on T_1-weighted images in the following regions: basal ganglia, subinsular region, global white matter, and temporal lobe according to a previously described 4-grade semiquantitative scale.[11] In addition, because of its extensive presence in NIT1-SVD, dPVS were also scored in the occipital lobe, cerebellum, and the mesencephalon. Normalized white matter hyperintensity volumes (nWMHv) were calculated by dividing total white matter hyperintensity (WMH) volume by the intracranial volume. nWMHv was available for 18 individuals heterozygous for the *NIT1* p.(Arg243Trp) variant and for 38 individuals heterozygous for a truncating *NIT1* variant.

Statistics

Total dPVS scores were compared between individuals heterozygous for a *NIT1* variant and age- and sex-matched controls from UK Biobank using a Wilcoxon rank sum test. To compare nWMHv between individuals heterozygous for a *NIT1* variant and the total number of 40,802 controls in UK Biobank, regression analysis was performed controlling for age and sex. To receive normal distribution of residuals, nWMHv was log transformed. All statistical analyses were performed in R.

Results

Genetics and protein prediction

All identified patients had bi-allelic variants in the *Nitrilase 1* gene (*NIT1*, OMIM 604618), located on chromosome 1q23.3, encoding the NIT1 enzyme. Patients were either compound heterozygous for the *NIT1* c.727C>T, p.(Arg243Trp) variant and the truncating *NIT1* c.198_199del, p.(Ala68*) variant, or homozygous for the *NIT1* p.(Arg243Trp) variant (Table 1 and Figure 1A and B). The *NIT1* p.(Arg243Trp) variant alters a strongly conserved residue (up to Baker's yeast) and was predicted to be pathogenic by in silico prediction programs. 3D modeling showed that the p.(Arg243Trp) variant is located at the interface of the NIT1 monomers comprising the dimeric NIT1 enzyme (Figure 1C). The truncating variant c.198_199del, p.(Ala68*) introduces a stop codon in exon 3, which is predicted to lead to nonsense-mediated decay of the truncated transcript.

Table 1 Genetic, clinical, and neuroimaging characteristics of *NIT1*-small vessel disease patients

Patient ID	1	2	3	4	5	6
Pedigree ID	F1:II-1	F1:II-2	F1:II-3	F2:II-1	F3:II-1	F4:II-1
Age at last clinical assessment	†56-60	56-60	†46-50	46-50	56-60	56-60
Sex	M	F	M	M	M	M
NIT1 genotype	p.[(Arg243Trp)]; [(Ala68*)]	p.[(Arg243Trp)]; [(Ala68*)]	p.[(Arg243Trp)]; [(Ala68*)]	p.[(Arg243Trp)]; [(Arg243Trp)]	p.[(Arg243Trp)]; [(Arg243Trp)]	p.(Arg243Trp)(;) (Arg243Trp)[f]
Clinical Characteristics (age at onset)						
Hemorrhagic stroke	+ (56-60)	-	+ (46-50)	+ (46-50)	-	-
Ischemic stroke	-	-	+[a]	+ (36-40)	+	-
Tremor	hands (36-40)	hands (36-40)	+[b]	-	hands[b]	-
Dystonia	neck (46-50)	right thumb and index finger[b]	+[b]	-	-	-
Chorea	-	right lower extremity (36-40)	-	left upper extremity[b]	-	bilateral upper and lower extremities[b]
Dysarthria	+ (46-50)	+[b]	+ (36-40)	+[b]	-	+[b]
Bradykinesia	+/−[b]	+[b]	-	+[b]	+[b]	+ (51-55)
Gait disturbance	+/−[b]	+ (56-60)	NA	-	+[b]	+ (51-55)
Syncope	+/−[c]	+ (46-50)	NA	+ (46-50)	+ (56-60)	-
Fatigue	+[b]	+[b]	NA	-	-	+[b]
Psychiatric symptoms	-	depression (41-45)	Psychosis[b]	-	-	-
Cognitive/memory impairment	+ (36-40)	+ (51-55)	Unknown	+ (36-40)	+[b]	+[b]
MOCA	NA	10/30 (56-60)	-	25/30 (46-50)	18/30 (56-60)	NA
Cardiovascular risk factors[d]	None	HC	HT, HC	HT, HC	None	None
Neuroimaging	MRI + CT	MRI	CT	MRI + CT	MRI	MRI
dPVS	+	+	+	+	+	+
WMH	-	+	Unknown[e]	+	+	+
Lacunes	-	+	Unknown[e]	+	+	-
Microbleeds	-	+	Unknown[e]	-	-	+
Hemorrhagic foci	+	+	Unknown[e]	+	-	+
Intracerebral hemorrhage	+	-	+	+	-	-

Age ranges are given to ensure patient anonymity. *HT*, hypertension; *HC*, hypercholesterolemia; *DM*, diabetes mellitus; *NA*, not available; *S*, smoking.

[a]Traumatic occlusion of the right internal carotid artery at age 16 to 20 years with left-sided hemiparesis with almost full recovery, spontaneous recanalization. Recurrence ischemic stroke right hemisphere at 36 to 40 years. Magnetic resonance angiography was reported to show an accessory artery originating from the distal carotid artery, suggested to be an arteriovenous malformation.

[b]Age of onset not reported.

[c]Although syncope was not reported, significantly increased sleep tendency with sudden narcolepsy-like sleep attacks was described.

[d]Hypertension (HT), hypercholesterolemia (HC), Diabetes Mellitus (DM), smoking (S)

[e]Could not be assessed on the CT scan made after ICH; MRI was not available for this patient.

[f]A deletion of *NIT1* on 1 of the alleles was excluded in patient 4 and 5, but not in patient 6.
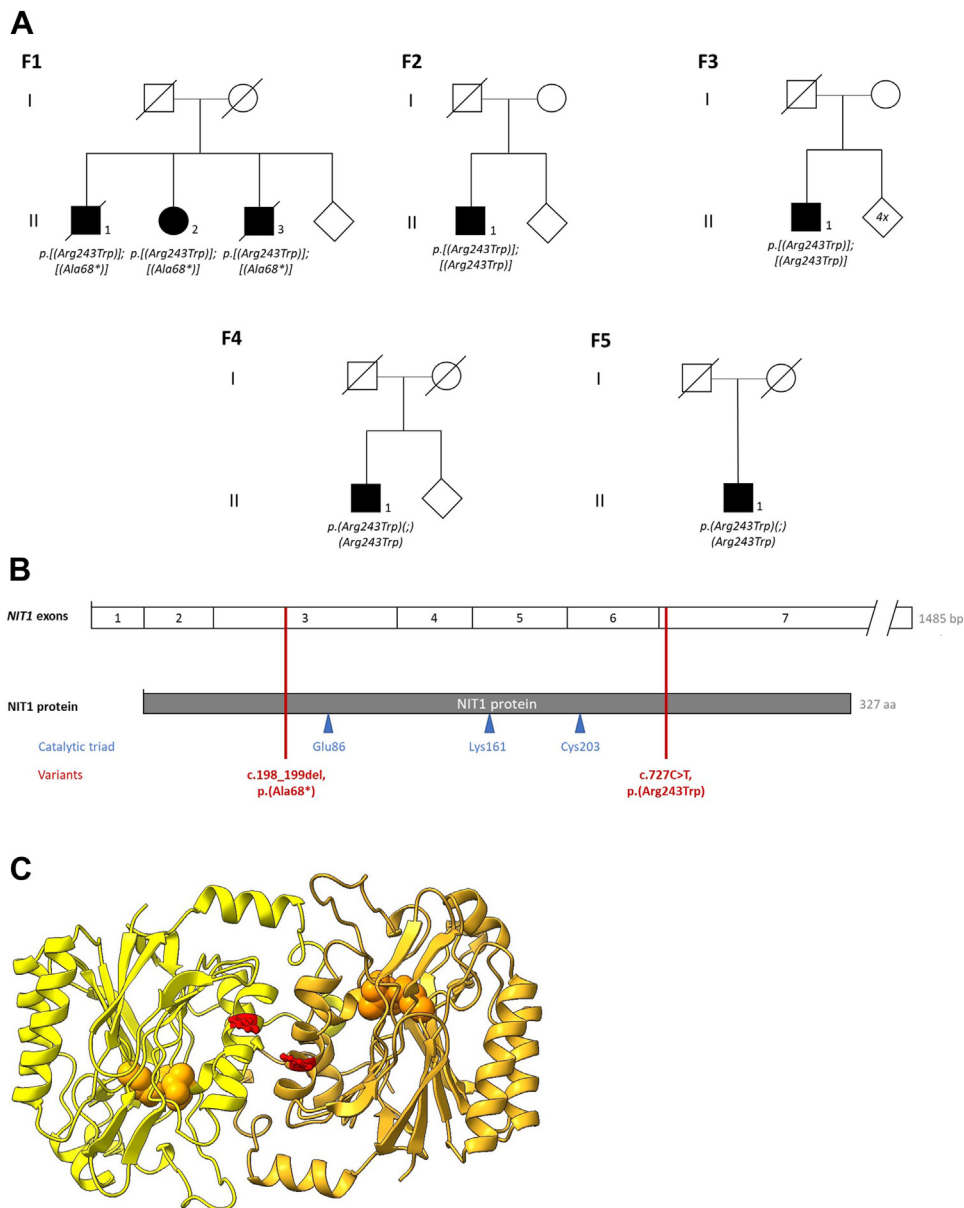
Figure 1 **_NIT1_ variants detected in 5 unrelated pedigrees and 3D protein modeling.** A. Simplified pedigrees of the NIT1-small vessel disease patients identified in this study. B. Schematic representation of the _NIT1_ exons and NIT1 protein, including the location of the amino acids composing the catalytic triad and the _NIT1_ variants found in the patients in this study. C. 3D modeling of the homodimeric NIT1 enzyme. The p.(Arg243Trp) substitution (shown in red) is located at the interface of the 2 NIT1 monomers. Spheric residues indicate the catalytic site of each monomer (Glu86-Lys161-Cys203).

Clinical and neuroimaging phenotype

Clinical characteristics of 6 out of the 7 patients with bi-allelic _NIT1_ variants are summarized in Table 1. Cardinal clinical features included progressive movement disorders, such as dystonia, chorea, bradykinesia, and tremor, as well as gait disturbance and dysarthria, not as a direct consequence of an evident ischemic or hemorrhagic stroke. Slowly progressive cognitive decline was another consistent feature. Two patients died because of massive non-lobar ICH, between age 45 and 60 years. Three patients had a history of ischemic stroke. All patients shared a distinct neuroimaging phenotype (Figure 2), with an extremely high burden of dPVS in both supratentorial and infratentorial brain regions. dPVS were especially prominent in the basal ganglia and thalamus, leading to a honeycomb appearance of the deep gray matter. dPVS were present to a lesser extent in the mesencephalon, pons, and cerebellum and in the temporal, occipital, and parietal lobes (Supplemental Table 1). The burden of white matter hyperintensities varied between patients, even of the same age. Half of the patients had lacunes on MRI. In 3 patients, hemorrhagic foci in the basal ganglia were seen, located between clusters of
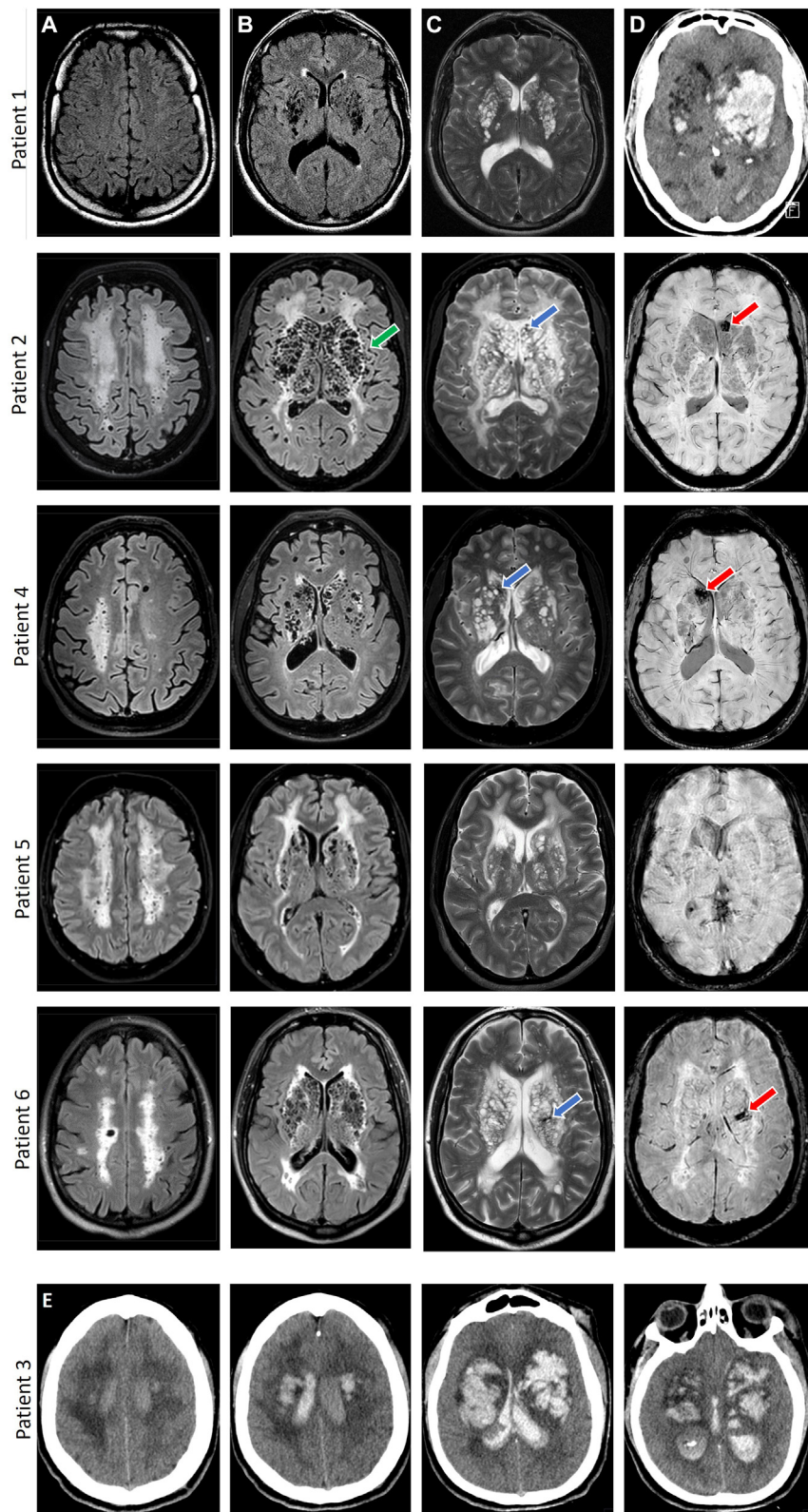
Figure 2   Neuroimaging abnormalities in 6 patients with NIT1-small vessel disease from 4 different pedigrees. A and B. T2-FLAIR and (C) T2-weighted images of patients 1, 2, and 4-6 showing numerous and massively dilated PVS in the basal ganglia-thalamus complex, leading to a honeycomb appearance of the deep gray matter, most striking in patient 2 (green arrow). dPVS were also present in other brain regions, including the centrum semiovale. The burden of white matter hyperintensities (WMH) varied, from only periventricular capping to confluent, symmetrical WMH also involving the external capsules. One patient had WMH in the anterior temporal lobes, and 1 patient had unilateral WMH, after hemorrhagic stroke (C1). D. SWI MR images (patients 2, 4, and 6) showing artefacts indicative of hemosiderin

dPVS. Neuroimaging (CT) at the time of fatal ICH showed massive hemorrhage in the basal ganglia complex, with intraventricular extension.

Brain small vessel pathology

The deeper lying perforating arteries and arterioles of the cerebrum, basal ganglia, and brain stem showed strongly abnormal vessel wall morphology (Figure 3A). There was a thickened media with abundance of hyalin and fibrin. Vessels were negative for Congo Red, Beta Amyloid, and NOTCH3 staining but did show large amorphic deposits, which stained positive for Periodic acid-Schiff and Toluidine Blue. On electron microscopy, pronounced electron-dense deposits were seen in the media and adventitia (Figure 3B). Often, these deposits were surrounded by fibrillar collagen. Immunohistochemistry showed reduced NIT1 staining of the larger arterioles and brain parenchyma in patients compared with controls (Figure 3C).

NIT1 expression and function in patient-derived fibroblasts and urine

Western blot analysis of patient fibroblasts showed a complete absence of NIT1 protein in all patients, including patients homozygous for the p.(Arg243Trp) missense variant (Figure 4A). Fibroblasts of unaffected relatives heterozygous for the p.(Arg243Trp) variant showed a trend toward lower NIT1 protein levels. To determine whether the c.727C>T; p.(Arg243Trp) variant leads to aberrant splicing and thereby a premature stop codon, RNA-seq was performed. This did not show aberrantly spliced NIT1 transcripts (Supplemental Figure 1A). Gas chromatography-mass spectrometry analysis of urine samples showed increased levels of dGSH, confirming the loss of NIT1 enzymatic activity (Figure 4B and C). Transcriptomic analyses did not reveal altered expression profiles of genes involved in pathways previously implicated in NIT1 function, ie, the glutathione pathway and the TGF beta and WNT signaling pathways (Supplemental Figure 1B).

NIT1 variant frequency and estimated NIT1-small vessel disease prevalence

The NIT1 c.727C>T; p.(Arg243Trp) variant had a frequency of ~1/2000 in UK Biobank. In gnomAD, the frequency of the p.(Arg243Trp) variant was ~1/4000; p.(Arg243Trp) was present in the non-Finnish European and African/African American individuals but not in South and East Asian or Ashkenazi Jewish individuals. NIT1

p.(Arg243Trp) frequency was highest in a Dutch population database (GoNL), namely, 1/500. The frequency of truncating NIT1 variants was ~1/1000 in the various population databases, and truncating NIT1 variants were seen in individuals from all ethnicities in gnomAD. Based on these frequencies, the minimal estimated prevalence of NIT1-small vessel disease in The Netherlands is 1/450,000 and worldwide ~1/1,800,000. This would mean minimally 40 patients with NIT1-small vessel disease in The Netherlands and minimally 4500 patients worldwide. The 7 Dutch patients were from different regions of The Netherlands, did not come from a genetic isolate, and their parents were not known to be consanguineous.

Individuals heterozygous for a NIT1 variant do not have a clinical or neuroimaging phenotype

Individuals found to be heterozygous for a NIT1 truncating or p.(Arg243Trp) variant in UK Biobank (UKB cases), did not have a NIT1-SVD clinical or neuroimaging phenotype. None of the UKB cases had neuroimaging evidence of ICH or a medical history of ICH. Ischemic stroke frequency was lower in UKB cases compared with the whole UKB population (1,04 % vs 2,58%). UKB cases heterozygous for the NIT1 p.(Arg243Trp) variant showed a slight increase in total burden of dPVS compared with controls, but this did not reach statistical significance ($P = .055$) (Figure 5A). There was no difference in dPVS burden between UKB cases heterozygous for a NIT1 truncating variant and controls. The neuroimaging burden of nWMHv also did not differ between UKB cases and controls (Figure 5B).

Discussion

Here, we report a novel genetic cause of cerebral small vessel disease caused by bi-allelic NIT1 loss-of-function variants. Patients have striking neuroimaging features, with numerous and strongly dilated perivascular spaces, resulting in a pathognomonic honeycomb appearance of the basal ganglia-thalamus complex. Brain vessels of patients show extensive electron-dense deposits located at the border zone of the media and adventitia. NIT1-small vessel disease (NIT1-SVD) is the first autosomal recessive disorder in which adult-onset ICH is a cardinal feature. The autosomal recessive inheritance can mask the genetic nature of the disorder because patients often present as apparently sporadic cases. However, the distinctive neuroimaging phenotype enables a spot-diagnosis, and after ascertaining the initial Dutch pedigree, multiple additional cases were recognized in our center based on brain MRI.

---

deposits in the basal ganglia (red arrows). These correspond to hypointense lesions located between clusters of dPVS (hemorrhagic foci) on T2-sequences (blue arrows). Only a few small focal SWI artefacts suggestive of microbleeds were present in a minority ($n = 2$) of the cases (not shown). D and E. CT images of patients 1 and 3 showing massive bilateral hemorrhage in the basal ganglia with breakthrough into the lateral ventricles.
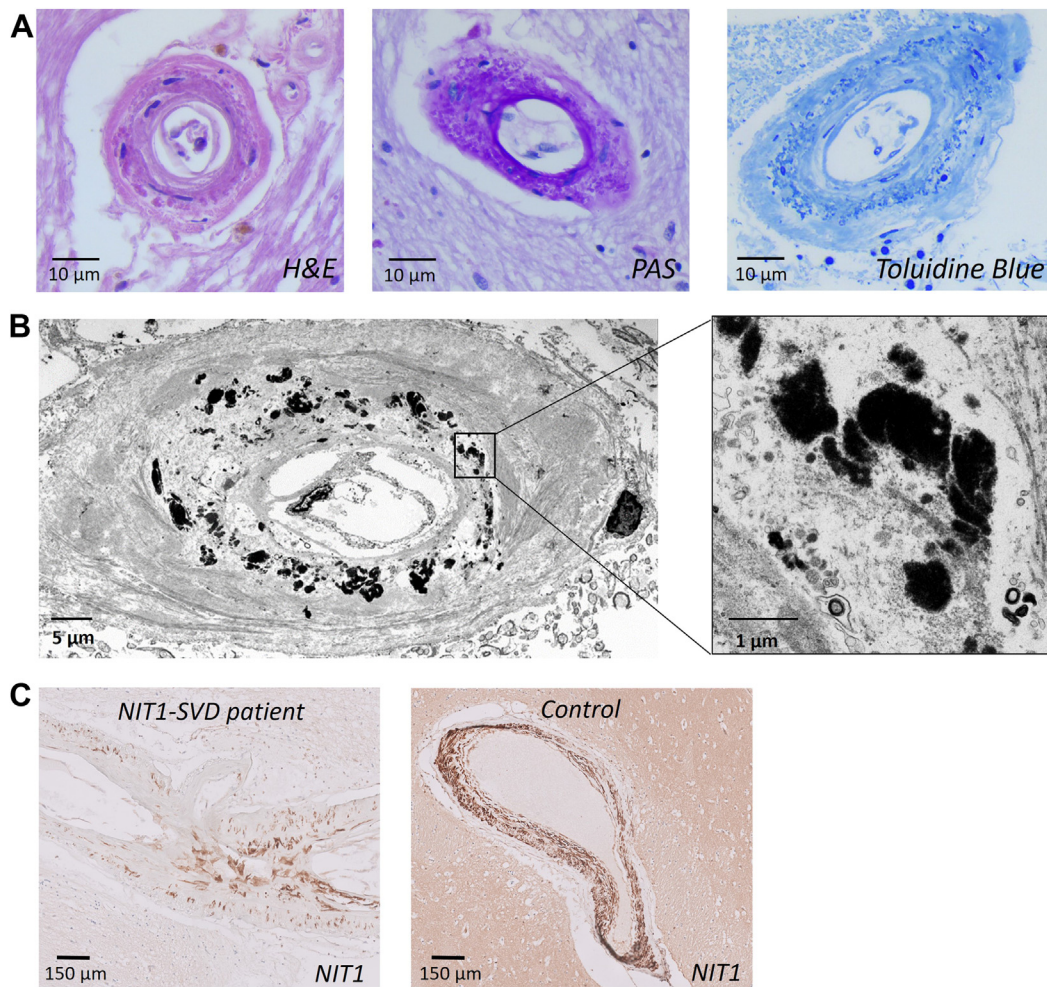
Figure 3   Small vessel wall pathology. A. Hematoxylin-eosin staining of brain vessels of the 2 deceased patients (patients 1 and 3), showing a thickened media and adventitia with deposits of granular material in the outer layers and fibrosis and hyalinization of the more inner layers. Periodic acid-Schiff and toluidine blue stain of vessels highlighting the deposits of granular material. B. Electron microscopy of brain vessels showed numerous electron dense deposits in the media and adventitia in both patients. Often these deposits were surrounded by fibrillar collagen. C. NIT1 immunohistochemistry on brain tissue of NIT1-SVD patients (compound heterozygous for *NIT1* variants p.(Arg243Trp) and p.(Ala68*)) showed reduced NIT1 staining in the larger arterioles and brain parenchyma compared with controls. Representative images are shown.

Cardinal clinical features of NIT1-SVD are progressive mid-adult-onset movement disorders, cognitive decline and (fatal) deep ICH. Approximately 20 years before ICH, patients with NIT1-SVD present with movement disorders such as dystonia, chorea, bradykinesia and tremor, gait disturbance, or dysarthria. In addition, slowly progressive cognitive impairment is a key feature. Other reported symptoms include ischemic stroke, extreme fatigue, syncope, and psychiatric disturbances. The most striking and consistent MRI feature is the honeycomb appearance of the basal ganglia-thalamus complex, because of numerous strongly dilated perivascular spaces. These can be accompanied by hemorrhagic foci seen on susceptibility-weighted imaging, located between the clusters of dPVS. Most, but not all patients, have lacunes and extensive confluent periventricular and deep white matter hyperintensities. Notably, in contrast to cerebral amyloid angiopathies, microbleeds were not a consistent feature, with only 2 patients having a few microbleeds.

Patients were homozygous for the *NIT1* p.(Arg243Trp) missense variant or compound heterozygous for the *NIT1* p.(Arg243Trp) variant and the *NIT1* p.(Ala68*) truncating variant. We found a complete absence of NIT1 protein in patient fibroblasts on western blot, both in the compound heterozygous patients and the homozygous patients. Patients had increased levels of dGSH in urine, reflecting NIT1 loss of function.[2,6] The p.(Ala68*) variant is predicted to result in nonsense-mediated RNA-decay. How the p.(Arg243Trp) variants leads to absence of NIT1 protein is unclear. We excluded an effect on splicing via RNA-seq analysis. The p.(Arg243Trp) variant is located at the interface of the 2 NIT1 monomers. Speculatively, the variant affects the stability of the dimer, thereby leading to protein degradation.

NIT1 encodes the highly conserved 36 kDa NIT1 protein. The role of NIT1 in diverse biological processes has been incompletely clarified. What is known, is that NIT1 acts as a repair enzyme of the metabolic waste product of glutathione

Figure 4   Reduced NIT1 expression and function. A. Western blot showing absence of NIT1 protein expression in skin-derived fibroblasts from NIT1-SVD patients, both in patients compound heterozygous for the p.(Ala68*) and the p.(Arg243Trp) variant and in patients homozygous for the p.(Arg243Trp) variant. Unaffected relatives heterozygous for the p.(Arg243Trp) variant showed a trend toward reduced NIT1 expression compared with controls, which varied between experiments. Graph shows summary data of NIT1 protein levels from 2 independent experiments. Per experiment, the average NIT1 protein level in the controls was set to 1 as a reference. B. GC-MS analysis of urine of patients 2 and 4 showing the presence of the dGSH derivative. Total ion current chromatograms were aligned with respect to retention time. The dGSH derivative was not detectable in unaffected heterozygous family members. C. Mass spectrum of the dGSH derivative peak. The spectrum is essentially identical to the spectrum of purified dGSH.[3]

metabolism, dGSH.[3] NIT1 has also been suggested to act as a tumor suppressor via activation of the TGFβ-Smad and WNT signaling pathways.[2,4,5] These pathways were not up- or downregulated in the fibroblast transcriptomes of the NIT1-SVD patients. Moreover, the currently known functions of NIT1 cannot readily explain the pathological vessel wall changes with electron-dense protein deposits in the cerebral small arteries of NIT1-SVD patients, suggesting a novel function of NIT1 in vessel wall homeostasis. The appearance of the deposits on electron microscopy imaging was strongly reminiscent of the granular osmophilic material seen in patients with Cerebral Autosomal Dominant Arteriopathy with Subcortical Infarcts and Leukoencephalopathy (CADASIL),[12] but the deposits in NIT1-SVD were more abundant, larger, and less clearly associated with the basal membrane of the vascular smooth muscle cells.

The co-occurrence of dPVS and ICH in NIT1-small vessel disease patients supports the recently described association between dPVS and increased risk of ICH.[13,14] PVS are physiological spaces surrounding small vessel walls as they run from the subarachnoid space through the brain parenchyma. dPVS are a neuroimaging feature of small vessel disease,[15] speculated to reflect impaired clearance of cerebrospinal fluid and/or metabolic waste.[16] The massively dilated PVS in NIT1-SVD may be caused

by increased levels of metabolic waste products as a consequence of NIT1 loss of function, exacerbated by the extensive vessel wall pathology leading to impaired glymphatic clearance.[17]

Family members and UK Biobank cases heterozygous for a *NIT1* pathogenic variant did not have a NIT1-SVD clinical or neuroimaging phenotype, and family members did not have increased levels of dGSH in urine. UK Biobank cases heterozygous for the *NIT1* p.(Arg243Trp) variant had a slightly increased dPVS burden compared with UK Biobank controls; therefore, some effect of *NIT1* p.(Arg243Trp) variant heterozygosity on brain small vessel physiology cannot be ruled out, although this is likely not of clinical relevance, as none of the heterozygous UK Biobank cases or heterozygous family members of NIT1-SVD patients suffered from movement disorders, cognitive decline, or ICH. Based on frequencies of the *NIT1* p.(Arg243Trp) variant and *NIT1* truncating variants in UK Biobank and gnomAD, we calculated that an estimated minimum of 4500 individuals worldwide are affected with NIT1-SVD. In this calculation, we only took into account the p.(Arg243Trp) variant, but other *NIT1* (missense) variants, for example, those located in the catalytic triad (Glu86-Lys161-Cys203), may also lead to loss of NIT1 function, in which case the prevalence of NIT1-SVD would be higher.

Figure 5 **dPVS and nWMHv load in individuals heterozygous for a *NIT1* variant in UK Biobank compared with controls and NIT1-SVD patients.** Individuals found to be heterozygous for a *NIT1* truncating or p.(Arg243Trp) variant in UK Biobank (UKB cases), did not have a NIT1-SVD neuroimaging phenotype. A. UKB cases heterozygous for the *NIT1* p.(Arg243Trp) variant had a borderline significant increase in dPVS burden compared with age- and sex-matched controls. Total dPVS burden did not differ between UKB cases with a truncating *NIT1* variant and controls. B. There was no difference in nWMHv between UKB cases and controls.

In conclusion, we describe a novel cause of genetic cerebral small vessel disease characterized by movement disorders, progressive cognitive decline, a highly distinct neuroimaging phenotype of dilated perivascular spaces, and deep brain hemorrhage, caused by bi-allelic *NIT1* loss-of-function variants.

Data Availability

The data that support the findings of this study are available from the corresponding author, (J.W.R.), upon request.

Acknowledgments

Funding

Author Information

Conceptualization: J.W.R., G.G., S.A.J.L.O.; Data Acquisition: J.W.R., M.N.C., K.L.D., A.A.M., J.V., R.I.K., S.T.d.B., K.M.v.N., H.J.B., H.W.B., G.J.G.R., C.R.J., S.G.v.D., E.A.R.N., G.G., S.A.J.L.O.; Data Analysis: J.W.R., M.N.C., K.L.D., A.A.M., J.V., M.K., R.I.K.,

L.H.M., G.J.G.R., F.B., C.R.J., S.G.v.D., E.A.R.N., G.G., S.A.J.L.O.; Writing-original draft: J.W.R., M.N.C., G.G., S.A.J.L.O.; Writing-review and editing: K.L.D., A.A.M., J.V., M.K., R.I.K., S.T.d.B., K.M.v.N., H.J.B., H.W.B., L.H.M., G.J.G.R., F.B., C.R.J., S.G.v.D., S.G.v.D., E.A.R.N.

Ethics Declaration

This study has been approved by the Medical Ethics Committee Leiden The Hague Delft (P21.013). Written informed consent for publication was obtained from all patients. Data have been deidentified for publication. Studies were performed in accordance with the Declaration of Helsinki.

Conflict of Interest

The authors declare no conflicts of interest.

Additional Information

The online version of this article (https://doi.org/10.1016/j.gim.2024.101105) contains supplemental material, which is available to authorized users.

Affiliations

[1]Department of Clinical Genetics, Leiden University Medical Center, Leiden, The Netherlands; [2]Department of Pathology, Leiden University Medical Center, Leiden, The Netherlands; [3]Department of Cell and Chemical Biology, Leiden University Medical Center, Leiden, The Netherlands; [4]Department of Radiology, Leiden University

Medical Center, Leiden, The Netherlands; [5]Department of Neurology, Leiden University Medical Center, Leiden, The Netherlands; [6]Department of Neurology, St Jansdal Hospital, Harderwijk, The Netherlands; [7]Department of Neurology, Amsterdam University Medical Center, location Vrije Universiteit Amsterdam, Amsterdam, The Netherlands; [8]Department of Biomedical Data Sciences, Leiden University Medical Center, Leiden, The Netherlands; [9]Department of Clinical Genetics, Erasmus Medical Center, Rotterdam, The Netherlands

References

1. Ekkert A, Šliachtenko A, Utkus A, Jatužis D. Intracerebral hemorrhage genetics. *Genes (Basel)*. 2022;13(7):1250. http://doi.org/10.3390/genes13071250

2. Semba S, Han SY, Qin HR, et al. Biological functions of mammalian Nit1, the counterpart of the invertebrate NitFhit Rosetta Stone protein, a possible tumor suppressor. *J Biol Chem*. 2006;281(38):28244-28253. http://doi.org/10.1074/jbc.M603590200

3. Peracchi A, Veiga-da-Cunha M, Kuhara T, et al. Nit1 is a metabolite repair enzyme that hydrolyzes deaminated glutathione. *Proc Natl Acad Sci U S A*. 2017;114(16):E3233-E3242. http://doi.org/10.1073/pnas.1613736114

4. Lin C, Zhang J, Lu Y, et al. NIT1 suppresses tumour proliferation by activating the TGFβ1-Smad2/3 signalling pathway in colorectal cancer. *Cell Death Dis*. 2018;9(3):263. http://doi.org/10.1038/s41419-018-0333-3

5. Mittag S, Valenta T, Weiske J, et al. A novel role for the tumour suppressor Nitrilase1 modulating the Wnt/β-catenin signalling pathway. *Cell Discov*. 2016;2:15039. http://doi.org/10.1038/celldisc.2015.39

6. Rendu J, Van Noolen L, Garrel C, et al. Familial deep cavitating state with a glutathione metabolism defect. *Ann Clin Transl Neurol*. 2019;6(12):2573-2578. http://doi.org/10.1002/acn3.50933

7. Richards S, Aziz N, Bale S, et al. Standards and guidelines for the interpretation of sequence variants: a joint consensus recommendation of the American College of Medical Genetics and Genomics and the Association for Molecular Pathology. *Genet Med*. 2015;17(5):405-424. http://doi.org/10.1038/gim.2015.30

8. Jumper J, Evans R, Pritzel A, et al. Highly accurate protein structure prediction with AlphaFold. *Nature*. 2021;596(7873):583-589. http://doi.org/10.1038/s41586-021-03819-2

9. Faas FG, Avramut MC, van den Berg BM, Mommaas AM, Koster AJ, Ravelli RB. Virtual nanoscopy: generation of ultra-large high resolution electron microscopy maps. *J Cell Biol*. 2012;198(3):457-469. http://doi.org/10.1083/jcb.201201140

10. Bycroft C, Freeman C, Petkova D, et al. The UK biobank resource with deep phenotyping and genomic data. *Nature*. 2018;562(7726):203-209. http://doi.org/10.1038/s41586-018-0579-z

11. Yao M, Hervé D, Jouvent E, et al. Dilated perivascular spaces in small-vessel disease: a study in CADASIL. *Cerebrovasc Dis*. 2014;37(3):155-163. http://doi.org/10.1159/000356982

12. Gravesteijn G, Munting LP, Overzier M, et al. Progression and classification of granular osmiophilic material (GOM) deposits in functionally characterized human notch3 transgenic mice. *Transl Stroke Res*. 2020;11(3):517-527. http://doi.org/10.1007/s12975-019-00742-7

13. Tian Y, Wang M, Pan Y, et al. In patients who had a stroke or TIA, enlarged perivascular spaces in basal ganglia may cause future haemorrhagic strokes. *Stroke Vasc Neurol*. 2024;9(1):8-17. http://doi.org/10.1136/svn-2022-002157

14. Duperron MG, Tzourio C, Schilling S, et al. High dilated perivascular space burden: a new MRI marker for risk of intracerebral hemorrhage. *Neurobiol Aging*. 2019;84:158-165. http://doi.org/10.1016/j.neurobiolaging.2019.08.031

15. Wardlaw JM, Smith EE, Biessels GJ, et al. Neuroimaging standards for research into small vessel disease and its contribution to ageing and neurodegeneration. *Lancet Neurol*. 2013;12(8):822-838. http://doi.org/10.1016/S1474-4422(13)70124-8

16. Duperron MG, Knol MJ, Le Grand Q, et al. Genomics of perivascular space burden unravels early mechanisms of cerebral small vessel disease. *Nat Med*. 2023;29(4):950-962. http://doi.org/10.1038/s41591-023-02268-w

17. Wardlaw JM, Benveniste H, Nedergaard M, et al. Perivascular spaces in the brain: anatomy, physiology and pathology. *Nat Rev Neurol*. 2020;16(3):137-153. http://doi.org/10.1038/s41582-020-0312-z